Pulsed field recombination

C. Wesdorp,[1] F. Robicheaux,[2] and L. D. Noordam[1]
[1]*FOM Institute for Atomic and Molecular Physics, Kruislaan 407, 1098 SJ Amsterdam, The Netherlands*
[2]*Department of Physics, Auburn University, Auburn, Alabama 36849*
(Received 29 May 2001; published 13 August 2001)

The pulsed-field recombination scheme is used to recombine free electrons with Li^+ ions to produce neutral Li atoms in a high Rydberg state ($n \approx 180$). The experimental conditions are similar to the conditions under which antiprotons and positrons are recombined to produce cold antihydrogen. In the current experiments we have trapped electrons in a Penning trap ($B \approx 35$ mT). Subsequently these electrons were recombined with spatially separated Li^+ ions. The recorded efficiency is 2.0% versus 0.3% in previous experiments with atomic ions. Several experiments and simulations were performed to study the dynamics of pulsed-field recombination in more detail.

DOI: 10.1103/PhysRevA.64.033414 PACS number(s): 32.80.Rm, 78.60.−b, 79.70.+q, 11.30.Er

I. INTRODUCTION

Recombining a free electron and a free ion is not simple, since a third body is required to take away the excess kinetic energy. Several recombination schemes are proposed, such as a three-body recombination [1,2], dielectronic recombination, which can be seen as an inverse Auger process [2,3], radiative recombination, and stimulated radiative recombination [2,4]. Radiative recombination can be seen as the inverse of photoionization. These schemes have the disadvantage that high densities of charged particles at low temperatures are required, in order to achieve a sufficient recombination rate. Another recombination scheme, that relies on charge exchange with positronium was suggested by E. A. Hessels *et al.* [5]. This scheme is expected to yield a high recombination rate but so far this scheme is not realized in practice. In this paper, we will present a detailed study of a novel, controllable, and efficient recombination scheme [6,7].

In Fig. 1, the pulsed-field recombination (PFR) scheme is sketched. An ion is situated in a static electric field and is awaiting the electrons. The static electric field modifies the Coulomb potential such that a saddle point is created [Fig. 1(a)]. If an electron, pulsed out of the electron trap with a well-defined kinetic energy, passes over the saddle point in the modified Coulomb potential, it will take a small, but not negligible, amount of time to return to the saddle point and escape from the ion [Fig. 1(a)]. If the static field is turned off [Fig. 1(b)] before the electron returns to the saddle point, it will remain bound in a highly excited state [Fig. 1(c)]. In order to study PFR one needs electron pulses with a well-defined controllable energy, free ions with little kinetic energy, and the ability to quickly turn off the electric field in which the ions are situated. A Penning trap was used to trap the electrons, which confines a charged particle by the use of electric fields in combination with a magnetic field. The trap will be discussed below in Sec. II.

Recombination of an antiproton and a positron into an antihydrogen atom would enable the first high-precision comparison between neutral matter and antimatter. The ATRAP and ATHENA collaborations at CERN have the prestigious goal to produce cold (4 K) and trapped antimatter in order to compare a hydrogen atom with its complementary atom: the antihydrogen atom. Precise comparisons are a test for the *CPT* theorem that states that nature is invariant under the combined operations of charge conjugation, parity conjugation, and time reversal [8]. This means that every particle state must have an antiparticle state with equal mass, spin, and lifetime, but opposite magnetic moment, and charge. Moreover, gravity experiments on neutral antimatter can test the weak equivalence principle [9] which states that a particle behaves the same under the influence of gravity as an antiparticle. Neutral antimatter is required for these experiments since the smallest stray electric and magnetic fields already strongly influence charged antimatter particles.

With the technique of pulsed-field recombination (PFR) we have previously shown that it is possible to recombine free electrons and free atomic (rubidium) [6] or molecular (C_{60}) [7] ions in a controllable and efficient manner, and can in fact be seen as the inverse of pulsed-field ionization. From these results and the supporting theory, it was concluded that PFR can be used to recombine any sort of ion with a free electron and that it could also be used for the production of atomic antihydrogen. It was estimated that the PFR scheme could produce 10^2–10^3 antihydrogen atoms in the already realized combined trap for particles of opposite sign [10]. Moreover, it was shown that PFR can be used as a tool to produce Rydberg states in complex molecules [7] where Rydberg production by laser excitation fails. This opens up the way for cation spectroscopy of complex molecules by the technique of photoinduced Rydberg ionization (PIRI) [11] spectroscopy.

We report on experiments using ''ordinary'' matter to study the recombination dynamics of the PFR scheme. There were four major motivations for performing these experiments. The first is that in a typical PFR experiment, one uses the inertia of an ion (with respect to the small inertia of an electron) to enable an electron to approach the ion in a static electric field. One therefore might expect that a decrease in the efficiency is observed of the PFR scheme when one tries to recombine free electrons to ions with less mass (such as a proton). To test if the PFR scheme could indeed be used to recombine lighter ions with free electrons we have used lithium ions. Lithium, being 12 times lighter than rubidium

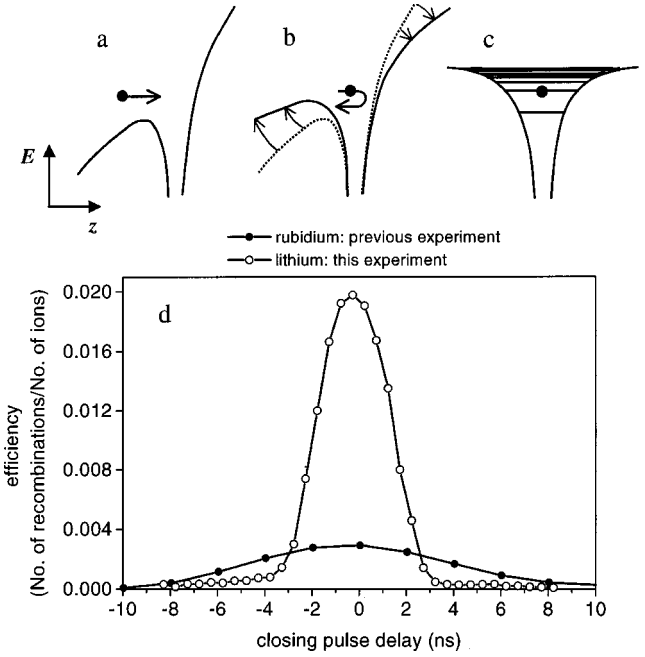

FIG. 1. Schematic representation of the pulsed field recombination scheme: (a) An ion awaits an electron in a static electric field, which is decelerated and has its turning point at the ion. (b) When the electron is at the turning point, the electric field is quickly ($\sim$1 ns) turned off. (c) If the field is turned off during the turning of the electron, a bound state is formed ($n \approx 180$). (d) Experimentally observed efficiency (number of recombined atoms divided by the number of free ions) as a function of the delay of the quick turn off. The open circles represent the data taken where we studied recombination of free electrons and lithium ions with the use of an electron trap. The solid circles represent data from previous work [6] where we studied recombination of free electrons and rubidium ions in a trapless geometry.

resembles much more a proton, although it is still 7 times heavier. The second motivation was that the previous experiments on PFR were performed in a geometry far different from the geometry used by ATRAP at CERN, where one will study recombination of *trapped* positrons and *trapped* antiprotons in Penning traps [12,13]. In the previous experiments, we produced electron pulses with a well-defined kinetic energy by photoionizing Li atoms in a static electric field by means of a narrow-band dye laser, instead of starting out from trapped electrons. Thus, in order to show that the PFR scheme can indeed be used in the geometry at CERN we have built an electron trap. A third motivation was to investigate what the effect is on a different total quantum defect of the recombined atoms on the recombination dynamics. It was stated [6] that PFR can be used to recombine any sort of ion with a free electron. Lithium has a total quantum defect of 0.452 ($\mu_0 = 0.4$, $\mu_1 = 0.05$, $\mu_2 = 0.002$) and rubidium a total quantum defect of 7.15 ($\mu_0 = 3.13$, $\mu_1 = 2.65$, $\mu_2 = 1.35$, $\mu_3 = 0.02$), a comparison of the previous experiments in rubidium with the current experiments in lithium could reveal a dependence of the recombination dynamics on the total value of the quantum defect. The last motivation was to increase the recombination efficiency of the PFR scheme.

We report on the detailed study of the recombination efficiency in a Penning trap configuration as a function of the temperature of the electrons in the trap and as a function of the storage time of the electrons in the trap. We also studied if a magnetic field in the range of 10–60 mT changed the recombination dynamics and the effect of a small residual electric field after the recombination event. A theoretical description using semiclassical calculations is presented. These semiclassical calculations give deeper insight into the states that are being formed in the recombination process and are used to probe the recombination dynamics not measurable by experiment.

II. SCHEME AND EFFICIENCY

In order to study PFR, one needs electron pulses with a well defined and controllable energy, free ions with little kinetic energy, and the ability to quickly turn off the electric field in which the ions are situated. The electron trap configuration allowed us to produce $\sim$4 ns electron pulses. This was achieved by filling the electron trap with electrons and then quickly opening the trap. In the current experiments, the electrons leaving the trap have a kinetic energy of 1.5 eV and are decelerated by a static electric field of 3.0 V/cm, such that the electrons have their turning point at the position of a lithium ion cloud. The time required for the electron to travel from the saddle point, to the lithium nuclei, and back to the saddle point is about 1 ns for the fields and energies used in this experiment. This time is comparable to the turn-off time of the static electric field (90%$\rightarrow$10% in 0.8 ns). In Fig. 1(d), the experimentally determined efficiency (number of recombined rubidium atoms divided by the number of free ions) of this scheme is depicted as a function of the delay of the fast field turn off. This delay is with respect to the time when the free electron has its turning point in the electric field. Clearly, a maximum number of recombination events is recorded at zero delay. A comparison with the previous experiments with rubidium ions shows clearly that the efficiency (3.0×10^{-3} [6]) has gone up by almost an order of magnitude (2.0×10^{-2}) and that the electron pulses are much shorter. The increase in efficiency is mainly due to the fact that the electron pulses are shorter in time (from 11 ns [6] to 3.8 ns) and that we had better control over the overlap volume of the ion cloud and the volume of the electron pulses. We achieved the highest efficiency (6%) so far when we used the PFR scheme to recombine free electrons with free ionic carbon clusters in a trapless environment [7]. Note that the results of Fig. 1(d) show that PFR can be used in geometry of trapped electrons and light ions.

III. EXPERIMENTAL REALIZATION

Our Penning trap consists of two stainless-steel parallel capacitor plates (thickness 1.0 mm) of 30.0 mm in diameter and two stainless-steel ring electrodes (thickness 0.5 mm) with an outer diameter of 30.0 mm and an inner diameter of 4.0 mm [Fig. 2(a)]. The two parallel capacitor plates (electrode 1 and 4) are separated by 5.0 mm and a hole of 10.0 mm was drilled through them covered by a grid, so that

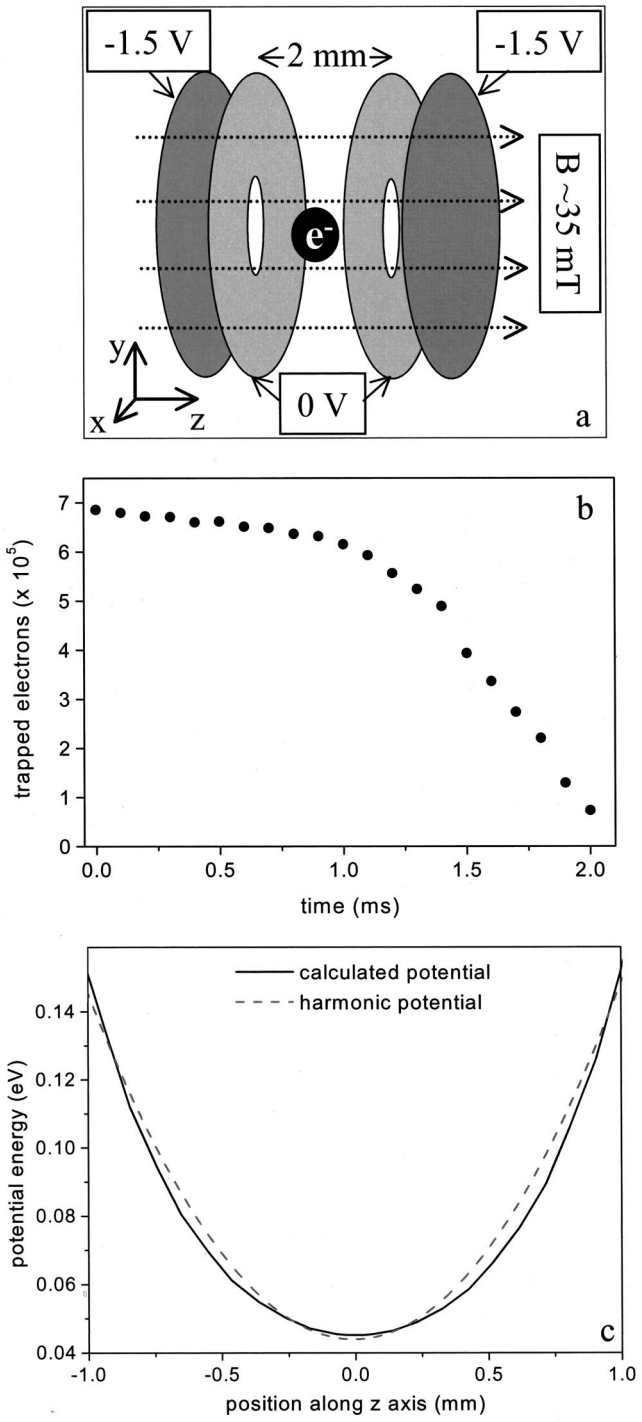

FIG. 2. (a) Schematic representation of the Penning trap, consisting of two flat capacitor plates and two ring electrodes. The lifetime of this trap was measured to be 1.5 ms at a background pressure of $\pm 10^{-6}$ Torr. (b) The number of trapped electrons as a function of the storage time. The lifetime was mainly affected by the background pressure. The minimum required magnetic field was 12 mT and increasing the magnetic field beyond this value hardly affected the lifetime of the trap. (c) Solid line: a calculation of the on-axis potential inside the Penning trap using SIMION, showing the harmonicity of the potential (dotted line: harmonic potential).

electrons could pass through these plates, but the plates still behave as flat capacitor plates. The two-ring electrodes were placed in between the parallel capacitor plates (electrode 2 and 3). The ring electrodes are separated from each other by 2.0 mm and each ring electrode was separated by 1.0 mm from the closest flat capacitor plate. A potential well was created in the z direction for electrons if the two parallel capacitor plates were biased with a negative voltage and the ring electrodes were biased with a higher voltage. In these experiments, the parallel capacitor plates were biased by a voltage of -1.5 V and the ring electrodes were biased in the range of 0.0 to -0.40 V. The minimum of the potential well was right in between the two ring electrodes, as shown by the SIMION potential calculation in Fig. 2(c). However, the electrons would still be able to escape the trap in the x-y direction. To prevent the electrons from escaping the trap in the x-y direction, a magnetic field of several tens of mT in the z direction was used. We have used SIMION to calculate the shape of the potential well on the z axis in order to design a plate configuration that produces as much as possible a harmonic potential in order to mimic the conditions of the ATRAP setup at CERN.

We filled the electron trap by photoionizing gas-phase lithium atoms. A jet of these alkali atoms comes from a resistively heated oven. The lithium atoms were ionized by means of two synchronized dye lasers pumped by the second harmonic of a Nd:YAG laser (532 nm), which produced laser pulses of about 7 ns duration with a repetition rate of 10 Hz. The first dye laser was used to excite the $2s$ electron to the $2p_{1/2-3/2}$ state in lithium (670.97 nm, 150 μJ) and the second dye laser (tunable from $340-350$ nm, 1.8 mJ per pulse) was used to drive the transition from the $2p$ state into the continuum. By connecting a fast-pulse generator on parallel capacitor plate 4 [Fig. 3(a)], the voltage could be switched from -1.5 V to $+1.0$ V within 1.0 ns on this plate. This enabled us to empty the trap at any time and record the electrons on a (Micro Sphere Plate) detector. Care was taken for correct impedance matching of the pulse generator to the electrode. In this way, the time dependence of the number of electrons at any time after the filling of the trap could be measured in a destructive way [Fig. 2(b)]. We were able to fill the trap with about $7(\pm 2)\times 10^5$ electrons and the recorded lifetime was about 1.5 ms determined by the background pressure ($\pm 10^{-6}$ Torr) in the vacuum chamber.

At 10.0 mm from the Penning trap plate configuration, another ring electrode was placed (electrode 5, outer diameter 30.0 mm, inner diameter 10.0 mm), which was used as the central electrode of an Einzel lens configuration. 10.0 mm after the Einzel lens again two parallel capacitor plates (electrodes 6 and 7) where situated separated by 5.0 mm. A hole of 10.0 mm was drilled through these parallel capacitor plates covered by a grid to minimize distortions on the electric field in-between these parallel capacitor plates. In between these parallel capacitor plates a homogeneous electric field was created of 3.0 V/cm. The first plate was connected to a ramp generator (Avtech, AV-1000-C) which could bias the plate from -5.0 to $+5.0$ V and ramp the voltage at a well-defined time from the bias voltage to $+10$ or -10 V, with a controllable slew rate (10%–90% in 5 ns to 1 ms). This voltage ramp was required to perform selective-field

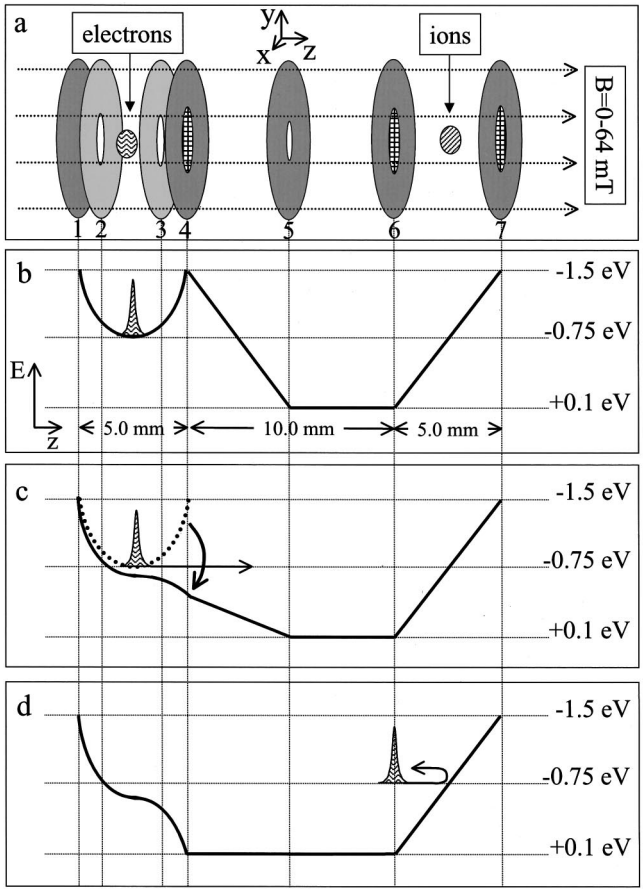

FIG. 3. (a) Experimental configuration. Two (micro sphere plates) detectors were used to record either electrons or ions. One detector was placed on the left of plate 1 to measure the number of trapped electrons in a destructive way. The other was placed on the right of plate 7 to measure how much ions were created before the recombination event and to measure electrons created from our recombined atom detection scheme. The first four plates on the left-hand side form the Penning trap. Note that grids are used to enable electrons to travel from one region to the other. The fifth plate is used as an Einzel lens. In between plate 6 and 7, ions are awaiting the electrons in a homogeneous electric field which could be quickly turned off by switching the voltage on plate 7. Plate 6 was connected to ramp generator in order to perform selective field ionization of the recombined atoms. (b)–(d) Schematic representation of the creation of electron pulses from the trap and their flight towards the ions.

ionization (SFI [14,15]) in order to measure how many recombined atoms were created and in which Rydberg state (discussed below). The last plate (electrode 7) was connected to a fast pulse generator (SRS DG535) ramping the voltage down from -1.5 V to any voltage in between -1.5 V and $+1.0$ V within 1.0 ns. Again, care was taken to match the impedance of the parallel capacitor plate to the output of the fast-pulse generator. The complete plate configuration [Fig. 3(a)] was placed in the heart of 2 coils (outer diameter 12.5 cm) in the Helmholtz configuration producing a tunable magnetic field of 0.0–64.0 mT. This set-up enabled us to first trap electrons [Fig. 3(b)], then pulse the trap open so that the electrons acquired a well-defined kinetic energy and travel towards the Einzel lens [Fig. 3(c)], guide the electrons towards the two parallel capacitor plates so that they pass through the grid in the cathode plate of the two parallel capacitor plates, and finally slow down the electrons by the static electric field such that they would turn around halfway in between these parallel capacitor plates ± 80 ns after the trap was pulsed open [Fig. 3(d)]. During the turning of the electrons around the ion cloud, the voltage on the last capacitor plate is quickly decreased from -1.5 V to typically $+0.1$ V to recombine the electrons with the free ions by means of the PFR scheme. A small static electric field is left over in this region of 200 mV/cm to ensure that any unrecombined free electron is accelerated out of this region and to prevent the effect of ''trapping'' the electrons in the attractive potential of the ion cloud. For the volumes and densities used in the experiments, the electrons feel an attractive field of <50 mV/cm at the edge of these volumes. Such a low-density plasma is therefore not stable when the ion region is biased with an electric field of 200 mV/cm.

In between the parallel capacitor plates a second atomic beam of lithium atoms was directed by means of a resistively heated oven. Lithium ions were ionized either by using the same lasers to produce the electron pulses and aligning the beams on the second atomic beam (scheme I: used for experiments were the electrons were stored in the Penning for times shorter than 500 ns) or by using a third dye laser (scheme II: used for experiments were we studied the recombination efficiency as a function of storage time of the electrons in the trap) pumped by the second harmonic of a Nd:YAG laser, synchronized to the other two dye lasers. This laser produced 548.4 nm laser pulses with an energy of ± 10 mJ. The light was then frequency doubled in a potassium dihydrogen phosphate crystal that resulted in a collinear beam of 548.4 nm(± 9 mJ) and 274.2 nm(± 700 μJ). This collinear beam excited the $4p$ state in lithium by means of the 274.2 nm light and then ionized lithium atoms by driving the transition from this $4p$ state into the continuum. All the laser beams were created such that their diameter was 2 mm. Typically, we produced a cylindrically shaped ion cloud containing ~ 5000 ions, with a diameter of 2 mm and a length of 10 mm ($\rho_{ion} \approx 1.6 \times 10^5$ ions/cm^3).

IV. EXPERIMENTAL RESULTS

Timing is essential in a PFR experiment. This can be seen in Fig. 1(d): if we turn off the static electric field before the electrons reach the ions halfway between the parallel capacitor plates, the electrons will hardly be slowed down and will pass the ions without being recombined. If we turn off the static electric field too late the electrons will turn around at the ions but will gain kinetic energy again due to the static electric field and will leave the ion region in the opposite direction without being recombined. If we turn off the static electric field at the moment the electrons turn we record a maximum recombination efficiency of 2.0%. From Fig. 1(d) the time profile of the electrons is retrieved since a Gaussian profile is recorded with a width of 3.8 ns. This means that electron pulses of 3.8 ns were created. The electron pulses

are produced by pulsing open the electron trap in 0.8 ns, and therefore, one can expect that initially electron pulses are created with a duration of 0.8 ns. The fact that the measured pulse duration is six times longer is mainly due to Coulomb repulsion that results in an enlargement of the electron cloud. The enlargement of the electron cloud is mainly restricted in the *z* direction, since the presence of the magnetic field prevents the cloud from enlarging up in directions perpendicular to the *z* axis. This, in turn, would result in different travelling times towards the ions and therefore in an additional broadening of the time duration of the electron pulses. Note that the time duration of the electron pulses is much shorter than in the previous experiments where the electron pulse duration was limited by the duration of the photoionizing laser pulses ($\sim$10 ns).

In order to study the effect of the temperature of the trapped electrons in the trap on the recombination dynamics, we have used scheme I to produce the ionic cloud containing $5(\pm 2)\times 10^2$ ions in a volume of $\sim 7.9\times 10^{-3}$ cm^3. The ion cloud was produced in a static electric field of 3.0 V/cm 2 ns after the electron trap was filled. We filled the electron trap by ionizing the lithium atoms 74 cm^{-1} above the ionization limit resulting in $7(\pm 3)\times 10^5$ trapped electrons with a kinetic energy of 0.9 meV ($\sim$100 K). At the instant the electron trap is filled, this kinetic energy results mainly in motion along the *z* direction since the polarization of the ionizing laser is along the electric field, and thus, electrons will mainly be emitted along the *z* axis. The bandwidth of the ionizing laser was less than 0.2 cm^{-1}, resulting in an additional energy spread of less than 0.3 K. However, the noise generated from the pulse generators and voltage supplies connected to the electrodes cannot be neglected and will have an effect on the temperature on the electron cloud ($\sim$10 K). We also filled the trap by directing the 348.0 nm beam on a metal plate so that high-kinetic energy ($>$1000 K) electrons with a large energy spread were created in random directions and $3(\pm 1)\times 10^5$ electrons were trapped. Then 300 ns later the trap was pulsed open producing 1.5($\pm$0.1) eV electron pulses that traveled towards the ions to be recombined. In Fig. 4, the efficiency as a function of the time delay of the quick turn off is depicted for the ''cold'' and ''hot'' photocathode electrons. Clearly it is seen that the highest efficiency was obtained for lower temperatures of the trapped electrons. The fact that the efficiency increases for lower temperatures of the trapped electrons can be understood as follows. Due to the low-energy spread, more electrons will have their turning point at the same time in the static electric field at the ion cloud, and thus, more recombined atoms are produced with the same number of ions. Moreover, if the kinetic energy in directions perpendicular to the *z* axis decreases, the cyclotron orbit of the electrons will decrease. As we will discuss below, this will increase the recombination efficiency.

One might expect that the storage time of the electrons in the trap can influence the recombination dynamics, since the motional behavior of the electron cloud in a trap is time dependent [13] and also heating effects from external noise on the plate electrodes can play a role. During the modest lifetime of 1.5 ms of our trap we have seen a decrease in

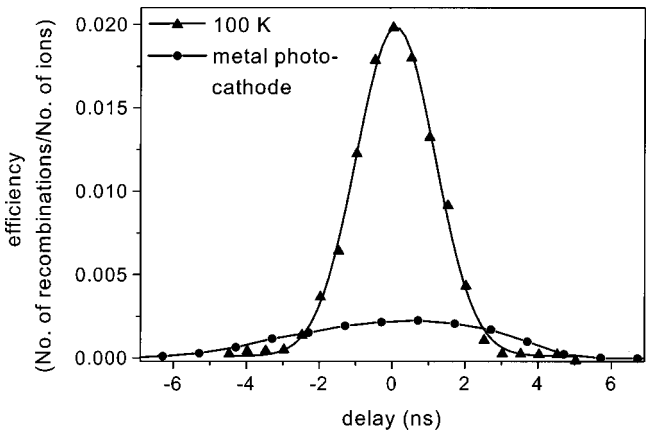

FIG. 4. The recombination efficiency as a function of the delay of the quick turn off. The triangles represent data where we filled the trap with electrons with a well-defined transverse kinetic energy. The circles represent data where we filled the trap with hot electrons with a very ill-defined kinetic energy (see text).

efficiency that cannot be fully attributed to the loss of electrons from our trap during longer waiting times. The behavior of the recombination dynamics on different storage times was investigated by producing ions with scheme II. In Fig. 5, the normalized time-delay profile is plotted for two different storage times (500 ns and 500 μs) showing that these profiles are identical. The recorded efficiency for a storage time of 500 ns was 2.0% and for 500 μs it decreased to 0.7%. We measured a 5–10% loss of electrons in the trap over the 500 μs waiting time, and thus, the 65% loss in efficiency cannot be attributed to just electron loss from the trap, since the number of recombined atoms scales linearly with the number of electrons in a electron pulse. A possible explanation is that heating effects of the electrons in the trap decrease the PFR efficiency, which will be discussed in more detail below.

A free electron is most likely to get recombined with the

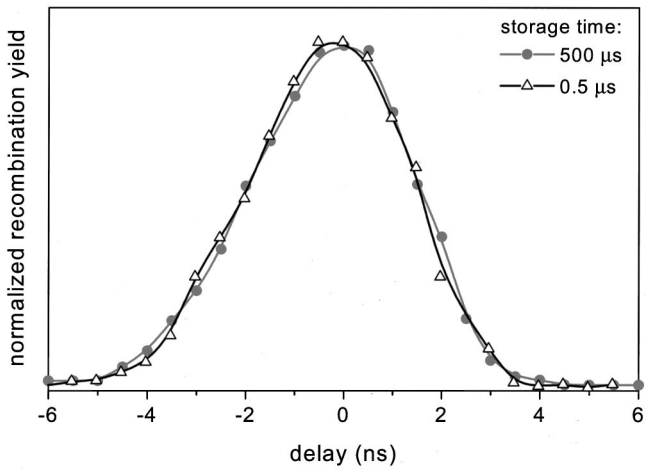

FIG. 5. The efficiency as a function for the delay of the quick turn off, for different storage times of the trapped electrons. The circles show the efficiency for a storage time of 500 μs and the triangles show the efficiency for a storage time of 500 ns.

PFR scheme when it is close to the nucleus with zero kinetic energy, but the coordinates (for a certain fixed distance to the ion) of the electron relative to the ion essentially do not play a role. This means that it is not appropriate to characterize PFR with a cross section as it is with most other recombination processes. Therefore, we introduced [6] the concept of an interaction volume (V_{int}) to describe the observed efficiency, which is the volume in space around the ion in which the electron has to be with a certain velocity to be recombined. A simple formula then predicts what this V_{int} should be

$$N_{rec}=\rho_e\rho_{ion}V_{overl}V_{int},$$

where N_{rec} is the number of recorded atoms [$10\pm(3)$], ρ_e is the electron density in the electron pulses, ρ_{ion} is the ion density [$6\pm(2)\times10^4$ cm^{-3}], and V_{overl} is the overlap volume of the electron cloud and the ion cloud. The size of V_{overl} is determined by the smallest cloud: the electron cloud. We thus obtain a V_{int} on the order of 10^{-10} cm^{-3}. Such an interaction volume would correspond to the space occupied by a Rydberg state around $n\approx180$. This suggests that high-Rydberg states are produced around $n\approx180$, by means of the PFR scheme. Below we discuss this interaction volume in more detail.

To verify this hypothesis, we used the technique of selective-field ionization (SFI), to probe the bound-state distribution after the recombination event. Every bound state in an atomic or molecular system has a static electric field associated with it by which it will be ionized. A highly excited state will be ionized by a relatively small electric field compared to a more deeply bound state. The relation between the value of the electric field at which field ionization classically occurs and the principal quantum number n state is (in atomic units)

$$F=\left(\frac{E}{2}\right)^2=\frac{1}{16n^4}. \quad (1)$$

There are deviations from this law depending how fast the electric field is ramped relative to the atomic or molecular dynamics, and the total value of the quantum defects of the atomic or molecular system [14,15]. If one ramps the static electric field in time and monitors at which time ionization occurs, one can deduce the bound-state distribution of an atomic or molecular system. Typically, we ramp the electric field with a slew rate of 1.70 V/cm per μs, from 0.20 to 5.0 V/cm. In Fig. 6, a SFI trace is depicted of the recombined states when during the recombination event, the electric field in the ion region is switched from 3.0 to 0.20 V/cm in 0.8 ns. The SFI detection started 1.4 μs after the recombination event. Clearly, it is seen that we mainly produce states that are ionized by the lowest SFI fields. If we use Eq. (1) to determine which bound states we have produced, we indeed observe that we are making Rydberg states with a principal quantum number around $n\approx180$, in perfect agreement with the principal quantum number we estimated from our observed efficiency and the V_{int} deduced from it. In Fig. 7, we show three SFI traces where we varied the residual electric

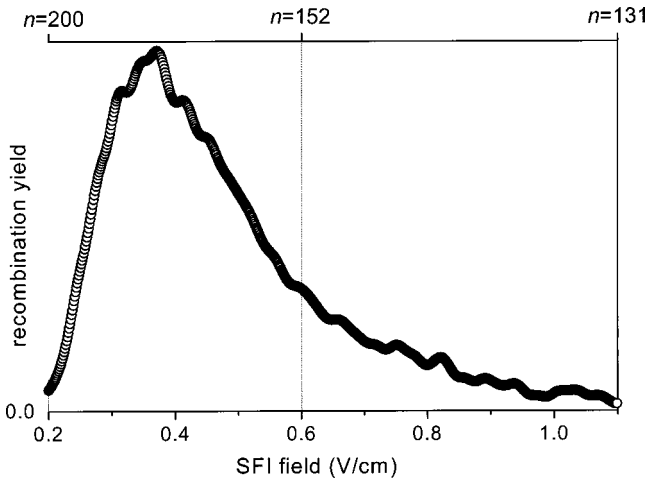

FIG. 6. The recorded state distribution by the technique of selective field ionization. Note that indeed states are created around $n=180$.

field after quick turn off. Similar states are produced, but we loose the highly excited states for stronger residual fields, which are unstable in the residual electric field.

We have also studied the effect of varying the magnetic-field strength on the PFR dynamics. This parameter could be varied over the range of 13 to 64 mT. For fields lower than 13 mT, the Penning trap would become unstable and the lifetime of the trap was strongly reduced. In Fig. 8(a), three different SFI traces are depicted for different magnetic fields. In Fig. 8(b), we plot the efficiency for various magnetic-field strengths. For higher magnetic fields, we record more recombined atoms. The increase in recombination efficiency can be explained by two effects. First, if one takes into account that the nonzero temperature of the electrons cloud introduces a nonfinite velocity in directions perpendicular to the z axis (transverse velocity). This means that for increasing tempera-

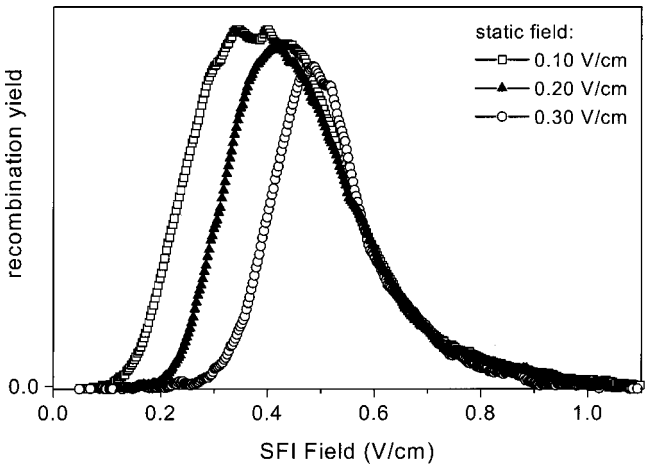

FIG. 7. The recorded state distributions for different values of the residual field after the recombination event. The open squares represent data for a residual field of 100 mV/cm, the solid triangles for a residual field of 200 mV/cm, and the open circles for a residual field of 300 mV/cm. It is clearly seen that an increase of residual field results in field ionization of the highest bound states.

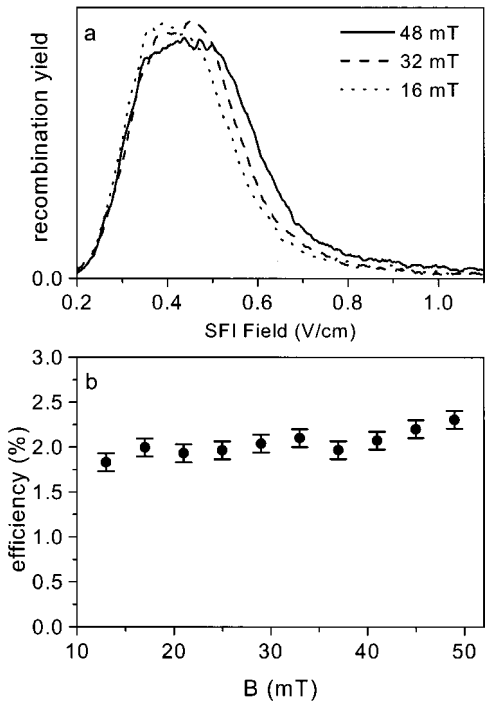

FIG. 8. (a) The recorded state distributions for different values of the magnetic field strengths. An increase in recombination efficiency is observed for higher magnetic field strengths. (b) Recombination efficiency as a function of the magnetic field strength.

tures of the electron cloud, this transverse velocity increases, and thus, the cyclotron orbit increases. If the radius of the cyclotron orbit becomes comparable or larger than the radius of V_{int}, the efficiency will decrease. This effect can be suppressed if the value of the magnetic field is increased since then the cyclotron orbit is reduced. The radius of V_{int} (10^{-10} cm^{-3}) is typically several micrometers (3 μm). The radius of the cyclotron orbit of the electrons can be estimated by: $r_c=\sqrt{2kTm}/eB$ and is also 3 μm if the transverse kinetic energy is 10 K in a field of 25 mT. The second effect increasing the efficiency can be that a stronger magnetic field guides the electrons better to the ions so that the number of electrons arriving at the ion cloud increases.

V. INTERACTION VOLUME

So far, we have discussed how the recombination efficiency can be understood in terms of an interaction volume that is an indication for the volume occupied by the created Rydberg state. Here, we discuss how a numerical estimate of V_{int} is obtained by classically solving Newton's equations. Given that the force is equal to: $\mathbf{F}(t)=q[\mathbf{E}(t)+\mathbf{v}(t)\times\mathbf{B}/c]$, one obtains an electron trajectory. The electric field ($\mathbf{E}$) is the superposition of the Coulomb potential of the ions and external field, $\mathbf{v}$ is the velocity of the electrons, and $\mathbf{B}$ is the magnetic field. We take the external field to be in the z direction so the force on the electron is in the negative z direction. The motion of the ion is neglected in this formulation and this neglect is the only major approximation in the calculation; when the cyclotron frequency of the electron is much lower than the Rydberg frequency, the main effect is the motional electric field from the center of mass motion, which is negligibly small for the parameters in this experiment.

Each individual electron trajectory is computed using a fourth-order Runge-Kutta algorithm with a variable time step that depends on the distance of the electron from the ion, with a smaller time step as r decreases. Because of the long-time propagations needed to obtain a theoretical SFI trace, no attempt was made to incorporate physical approximations into the numerical method. There were between 10^3 and 10^4 Rydberg periods for a typical run, which means the error in one Rydberg period needed to be held to much less than one part in 10^6.

There are two issues involved in calculating the interaction volume: (1) the initial distribution of positions and momenta and (2) the time propagation. In order to calculate the interaction volume, the ion is fixed at the origin while the electron is taken to have completely random positions in space and with Maxwellian distribution of velocities given by the temperature of the electrons. The time at which the electric field is ramped to zero is varied with a smaller time spacing compared to the time scale of the recombination phenomena ($\sim$1 ns). The interaction volume is calculated for each initial time of the electric field ramp using 2–4 thousand trajectories.

The only dependence on the ion was incorporated through an elastic scattering (as was stated in Ref. [6]) procedure for alkali ions. For alkali atoms, the electron was elastically scattered from its path for a pure Coulomb potential by changing the direction of the electron as it leaves the nucleus. The change was such to preserve the length of the Runge-Lenz vector, but to rotate it in the scattering plane by an amount given by 2π times the difference in quantum defects with angular momentum, $\mu_{\ell+1}-\mu_{\ell}$, for the angular momentum of the incoming electron. Because the electron scattered from the nucleus several times between the time of capture and the SFI field, the details of the scattering did not affect the calculation. It was only necessary that the scattering angle be of roughly the correct size. However, it was absolutely necessary to include some scattering for the calculations in very weak magnetic fields (10–40 gauss). The reason is that the classical motion separates for a H atom in a uniform electric field [14]. This means that the properties of the electron trajectory will not change at all for H after the ramp down, which is not true for the alkali atoms; the quantum defects cause a scattering between Stark states localized up field and states localized down field and we mimic this effect in the classical calculation by the elastic-scattering mechanism.

The interaction volumes calculated using this classical propagation gave results (calculated: $V_{int}=3\times10^{-10}$ cm^3) close to the experimentally determined ones (experiment: $V_{int}\approx10^{-10}$ cm^3). Although this agreement was promising, this is a single number and we felt that it was necessary to compare the experiment and calculation at a more detailed level to assure that the classical calculations were capturing the main features of the experiment. In order to do this, we directly compared the SFI signal from the experiment to that measured in the calculation, resulting in very good agree-

ment [6,7]. To this end, the calculations were extended in a straightforward manner. The calculation of a trajectory was performed as a single, very extended run. An electron's initial condition was chosen consistent with those in the experiment. The calculation was then run using Newton's equation to propagate the electron from the starting point to when it reached a point 10^6 a.u. down potential from the ion; the time it reached this point was taken to be the detection time. During the run, the electric field had a time variation that matched the time variation in the real experiment. The electric field starts at the initial value (typical value ~ 3 V/cm) and then is ramped down (typical value ~ 0.2 V/cm). After it is ramped down, the electric field is held constant for a long time (typical value ~ 1 μs) before being ramped at a constant rate for a long time (typical value ~ 1 μs). Any electron in the calculation that reaches the ''detector'' before the SFI field is ramped at ~ 1 μs is not counted as captured. The difficulty with the calculation was the long-time propagations that were needed to compute the SFI signal. The calculations were performed on a Beowulf cluster of ten Sun workstations constructed in the Auburn University Physics Department; this simulation was ideally suited for a parallel computer since it involved the results of many independent calculations [electrons with different starting conditions $x(t=0),\ p(t=0)$].

There were several general features of pulsed-field recombination that emerged from the calculation. One of the surprising features was that the core electrons played no role in the capture step of the recombination. This can be understood, since the core is so small that, essentially, every electron missed it during the capture step. On the other hand, the core dramatically changed the SFI signal by redistributing the electrons between up-potential and down-potential motion. Another interesting feature was that the SFI signal did not quantitatively predict the energy distribution of the captured electrons; the shape of the SFI signal was more strongly determined by the distribution of the Runge-Lenz vectors of the captured electrons at the start of the SFI ramp because the field ramp was fast compared to the time between elastic scattering of the electron at the core. Finally, the captured electrons were predominantly in states that were localized up potential just after the electric field was ramped down; the reason for this is that energy can be removed most efficiently from the electron plus ion system if the electron is on the up-potential side of the ion while the field is being ramped down. One of the consequences of this is that roughly half of the electrons are initially ''captured'' with an energy higher than the classical ionization threshold in the field. These electrons scatter into the down-potential direction and leave the ion before the SFI field can be ramped.

In Figs. 9–11, we show the results of calculations performed for an initial field of 3 V/cm that is ramped down to 0.2 V/cm. The functional form of the time varying part of the electric field is taken to be the $erfc(t/t_0)$ during the ramp down; the time width of the ramp is taken to be the duration to change from 90% of the initial E field to 10% of the initial E field. In all of the calculations, the magnetic field is taken to be 0 T and the temperature of the electrons is taken to be 0 K. While this does not exactly match any of the experimental parameters, the conclusions and the following discussion do not greatly change while it facilitates the calculation and the interpretation of the results.

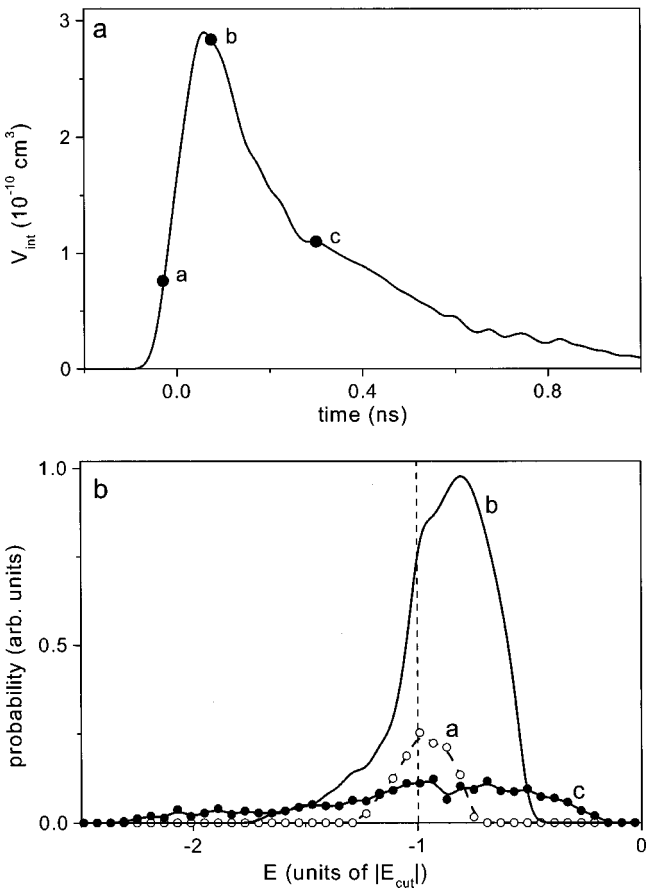

FIG. 9. (a) Calculated V_{int} for a 3 V/cm field ramped down to 0.2 V/cm over a time of 1/4 ns as a function of the time delay of the ramp. A smaller V_{int} is calculated for longer delay times. The markers a, b, and c are used in (b). (b) Calculated state distribution for different delay times (the markers a, b, and c correspond to the markers in (a). Each curve is normalized to give the correct relative recombination volume. $E/|E_{cut}|$ is the energy of the state divided by the classical ionization limit in a field of 200 mV/cm ($E_{cut} = 2\sqrt{F} = 1.25 \times 10^{-5}$ a.u.). Open dots: delay time $= -0.030$ ns. Solid line: delay time $= 0.075$ ns. Solid dots: delay time $= 0.300$ ns.

In Fig. 9(a), we show how the reaction volume depends on the time delay of the electric-field ramp compared to when an electron with zero energy would arrive at the ion in a *static* field; $t=0$. The width of the ramp is 1/4 ns. Note that there is no recombination if the ramp occurs at least 1/5 ns before the electron reaches the atom. The peak interaction volume is at times slightly greater than 0 ns because the electron needs to travel to the up-potential side of the atom to have the most energy removed. It is perhaps surprising that there is a substantial recombination for times much longer than both the ramp width and the time for a zero energy electron to travel from the saddle point around the nucleus and back to the saddle point. This comes from the electrons that have an energy only slightly larger than the initial saddle-point energy. These electrons take a very long time to

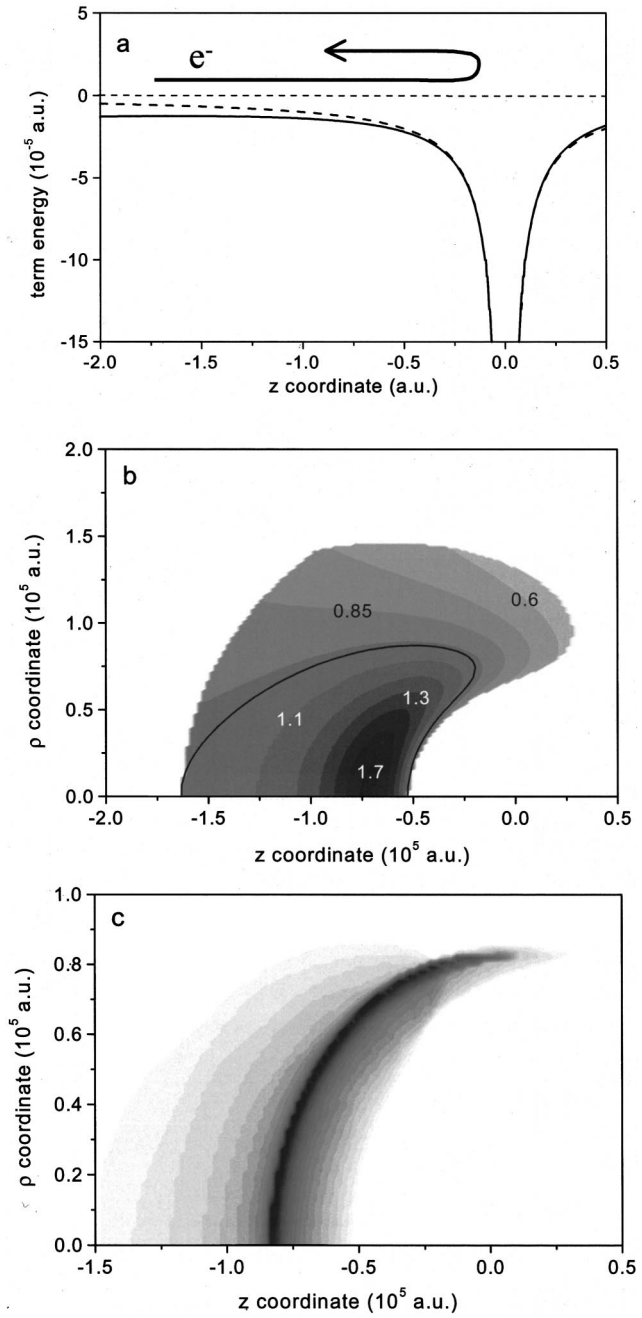

FIG. 10. (a) Dotted line: Coulomb potential. Solid line: modified Coulomb potential by an electric field of 200 mV/cm. (b) Contour plot of the energy of the recombined electron for t at the maximum recombination volume. The energy contours (E in units of $|E_{cut}|$) increase linearly from the contour near $z=-0.7\times10^5$ a.u. and $\rho=0$. The parameters ρ and z refer to the initial values of the electron trajectory. ρ is the initial distance of the electron from the z axis and z is the turning point the electron would have had with no electric field ramp and no ion. The thick line shows the division between electrons that recombine with energy below the classical ionization threshold and those above. (c) Contour plot of the recombination probability (divided by ρ to remove the dependence on the greater number of trajectories at fixed ρ) to any energy below the classical ionization threshold. The probability is obtained by integrating over all times of the ramp. The parameters ρ and z mean the same as in (b).

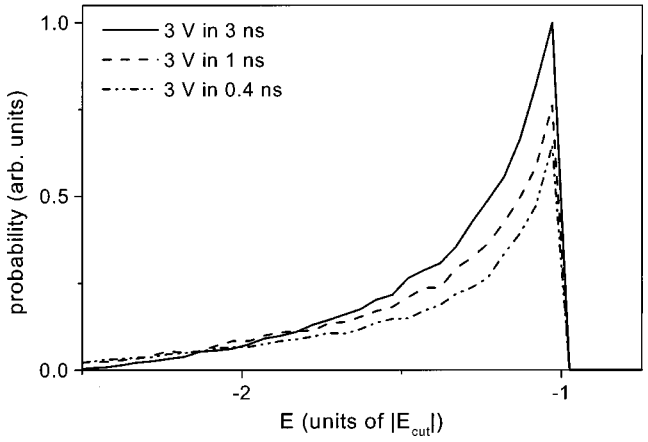

FIG. 11. The energy distribution of electrons recombined at any energy below the classical ionization threshold in a field of 200 mV/cm. The distribution is obtained by integrating over all times of the ramp. The solid line is the energy distribution for a ramprate of 3 V in 3 ns. The dashed line is the energy distribution for a ramprate of 3 V in 1 ns. The dash-dotted line is for a ramprate of 3 V in 0.4 ns.

travel over the classical saddle point; thus, they are still near the ion when the field is ramped down.

In Fig. 9(b), we show how the energy distribution of the recombined electrons vary with the time delay of the electric-field ramp. The energy distribution shows an enormous variation depending on the time delay of the ramp. For this calculation, an electron is counted as having recombined if it has not reached the detector within 50 ns after the end of the ramp. The electrons that recombine with energy greater than the classical ionization threshold ($E_{cut}=2\sqrt{F}=1.25\times10^{-5}$ a.u., and $F=200$ mV/cm), will scatter from the alkali core and leave the atom before the SFI field starts and will not be counted in the experiment; they are included in this figure so that the initial distribution after the ramp is presented in its entirety. The distribution at the early times give energy distributions that are peaked near the classical ionization threshold in a field of 200 mV/cm. Roughly half of the recombined electrons are at energies higher than the classical ionization threshold and will eventually elastically scatter from the core electrons and leave the ion. At later times, the distribution is flatter and have smaller contribution from above the ionization threshold.

Figure 10(a) depicts the potential of an ion in an electric field of 200 mV/cm (solid line) and zero field (dashed line) as a function of the z coordinate. In Fig. 10(b), we show the energy of the recombined electron as a function of parameters characterizing the starting position. The parameter ρ is the initial distance of the electron from the z axis and z is the turning point the electron would have had with no ramp and no ion [which can be related to Fig. 10(a)]. The rough size of the interaction volume can be estimated since the typical dimension is 10^5 a.u.$\sim0.5\times10^{-3}$ cm; this gives a interaction volume of roughly $(0.5\times10^{-3}\ \text{cm})^3\sim10^{-10}\ \text{cm}^3$. The solid line marks the division between the final energy being below the classical ionization threshold ($E<E_{cut}$, for a field of 200 mV/cm) and above the threshold; the electrons above

the threshold will elastically scatter from the core electrons and leave the ion. Since the electrons do not reach the ion core during the recombination step, this energy distribution is independent of the ionic species.

There are a number of features in Fig. 10(b) that can be understood at a qualitative level. For this discussion it is useful to remember that the force on the electron from the external field is in the negative z direction. The electrons that finish most deeply bound are on the z axis because these electrons can be in the most attractive part of the coulomb interaction when the field is ramped down. For the most part, the recombined electrons have a turning point at negative z. This is because the interaction of the electron with the ion is in the positive z direction for most of the trajectory, which pulls the electron to more positive z. Hence, the electron needs to be launched such that it will have a turning point short of the ion to be captured. This also explains why the contours go from lower to higher values of z as ρ increases; the effect of the Coulomb interaction decreases with increasing ρ, thus, the effect of the extra pull from the ion decreases, which means the value of the turning point should go towards the value without the ion: 0 a.u.

In Fig. 10(c), we show a plot of the probability for recombining on the ion (divided by ρ to remove the dependence on the greater number of trajectories with increasing ρ) to any energy below the classical ionization threshold obtained by averaging over all times for the ramp down. There is one interesting feature that was not apparent in previous graphs. In this figure there is a small region with high-recombination probability that starts near $z=-0.8\times10^5$ a.u. at $\rho=0$ and curves up as ρ increases. This line gives the initial conditions for an electron to have slightly more energy than is needed to go over the Coulomb plus static field barrier and approach close to the ion; an electron with this energy spends a long time going over the barrier because its velocity is small at the top of the barrier and is thus near the atom when the field is ramped down for any time of the ramp down.

In Fig. 11, we show the energy distribution of electrons recombined to energies below the classical ionization threshold as a function of the width of the ramped field. For this we average over all times for the ramp field. The width of the ramps are $\tau_1=1/4$ ns, $\tau_2=1$ ns, and $\tau_3=3$ ns. There are two features of interest. The energy distribution for the faster ramp rates have a larger energy fraction at the more deeply bound energies. This is what we expected since the amount of energy that can be removed from the electron is proportional to the time integral of $z(t)*[dF/dt]$. Therefore for a faster field ramp (larger dF/dt) there will be less chance that $z(t)$ changes sign, which would give rise to a result that partially cancels. The second feature is that the total interaction volume is slightly larger for the slower ramp rates (the ratio of the calculated interaction volumes is: $V_{int}(\tau_1):V_{int}(\tau_2):V_{int}(\tau_3)=1:0.85:0.68$); this result is counterintuitive and does not agree with experimental observations. The reason for the result in the calculation is that the slower ramp can be thought of as giving an initial field strength that is lower than the actual initial strength; since the distance scales are proportional to $1/\sqrt{F}$, the effective decrease in F gives slightly larger interaction volumes. Probably, this result is not seen in the experiment because electrons that are recombined near the classical ionization threshold are destroyed by nearby ions and passing electrons; if we count the recombination by counting trajectories at a fixed energy below the classical ionization threshold, then the calculated interaction volume decreases with increasing width of the ramp.

VI. DISCUSSION AND CONCLUSIONS

The fact that pulsed field recombination works with light atoms with different quantum defects indicates that indeed the PFR scheme is universal and is a promising scheme to recombine an antiproton and a positron. We have recorded an efficiency of 2.0% and demonstrated that PFR can in principle be implemented in a configuration where the charged particles are trapped and spatially separated. We have, however, not built an ion trap since the inertia of the ion (antiproton) compared to the electron (positron) is such that even in the static fields used in a PFR experiment (maximum field strength: 3 V/cm) the ions have hardly moved during the recombination event (±80 ns). Thus, one can load an ion trap, turn off the trapping potentials for 100 ns and turn them back on again with hardly loosing any ions from the trap, while performing the PFR scheme during the 100 ns. Another reason for not building an ion trap is that an ion trap uses inhomogeneous fields. We would however like to use homogeneous (time varying) electric fields after the recombination event to characterize in detail the recombined states we have produced.

The recombination efficiency was shown to depend on the transverse temperature of the electron cloud and magnetic-field strength where the highest efficiency was obtained for low temperatures of the electron cloud and high magnetic-field strengths. This was understood by the fact that a faster transverse motion will lead to larger cyclotron orbits. If the cyclotron orbit exceeds the interaction volume, the efficiency of the PFR scheme becomes less. We observed a loss in efficiency for longer storage times of the trapped electrons that is explained by electron loss and heating effects in the Penning trap.

A more detailed description was given about the interaction volume where we explained that the recombination probability is highest when high-Rydberg states are created. From the achieved efficiency and the introduced V_{int} it was concluded that Rydberg states with a principal quantum number of $n\approx180$ are created and this was verified by measuring the state distribution. We have shown that the use of a residual field gives control over the range of created Rydberg states.

The presented paper can be related to a previous observation of recombination using pulsed electric fields [16]. In these experiments unipolar ''half-cycle'' pulses [17] were used to recombine a free electron with its parent ion: a broad-band short (1.5 ps) laser pulse was used to ionize calcium atoms and shortly (~5 ps) after the ionizing pulse it was recombined again by a unipolar ''half cycle'' pulse. In the time domain, this process can be described as kicking the electron back to its parent ion, while in the frequency do-

main, it is a strong-field Raman transition between a virtual state in the continuum with a relative long lifetime and a bound state.

A last point worth noting is that to employ the PIRI technique [11] for molecular ion spectroscopy one needs a Rydberg state of a vibrationally cold molecule. In PIRI spectroscopy, a core electronic transition is photoexcited in a Rydberg molecule, which then decays by rapid autoionization. Because Rydberg molecules only weakly interact with optical radiation, the absorption wavelengths for a Rydberg molecule are very similar to those of the corresponding cation. In some cases it is not possible to create a Rydberg state in (complex) molecule by means of laser excitation. We have demonstrated that we can load an electron trap by means of ionization by a laser pulse, wait 500 μs, and then create a Rydberg state by recombining an ion and a free electron. This means that molecular ion spectroscopy can now be performed on species that were not accessible due to the failure of producing a Rydberg state by laser excitation. During the 500 μs storage time one has the opportunity to cool molecular ions to the vibrational ground state [18].

ACKNOWLEDGMENTS

C.W. and L.D.N. are supported by the Stichting Fundamenteel Onderzoek van de Materie (FOM) and the Nederlandse Organisatie voor Fundamenteel Onderzoek (NWO). F.R. is supported by the Chemical Sciences, Geosciences and Biosciences Division of the Office of Basic Energy Sciences, Office of Science, U.S. Department of Energy. We acknowledge EU-Network COCOMO, HPRNT-CT-1999-00129.

[1] G. Gabrielse, S. Rolston, L. Haarsma, and W. Kells, Phys. Lett. A **129**, 38 (1988); A. Muller, Comments At. Mol. Phys. **3**, 143 (1996).

[2] *Recombination of Atomic Ions*, edited by W. G. Graham, W. Fritsch, Y. Hahn, and J. A. Tanis (Plenum Press, New York, 1992); A. Müller and A. Wolf, Hyperfine Interact. **109**, 233 (1997).

[3] V. L. Jacobs, J. Davis, and P. C. Kepple, Phys. Rev. Lett. **37**, 1390 (1976); V. L. Jacobs and J. Davis, Phys. Rev. A **19**, 776 (1979); A. Müller *et al.*, Phys. Rev. Lett. **56**, 127 (1986); F. Robicheaux and M. S. Pindzola, *ibid.* **79**, 2237 (1997); L. Ko, V. Klimenko, and T. F. Gallagher, Phys. Rev. A **59**, 2126 (1999).

[4] F. B. Yousif *et al.*, Phys. Rev. Lett. **67**, 26 (1991); U. Schramm *et al.*, *ibid.* **67**, 22 (1991); R. Flannery, *Atomic, Molecular, and Optical Physics Handbook* (AIP Press, Woodbury, NY, 1996); M. L. Rogelstad, F. B. Yousif, T. J. Morgan, and J. B. A. Mitchell, J. Phys. B **30**, 3913 (1997).

[5] E. A. Hessels, D. M. Homan, and M. J. Cavagnero, Phys. Rev. A **57**, 1668 (1998).

[6] C. Wesdorp, F. Robicheaux, and L. D. Noordam, Phys. Rev. Lett. **84**, 3799 (2000).

[7] C. Wesdorp, F. Robicheaux, and L. D. Noordam, Chem. Phys. Lett. **323**, 192 (2000).

[8] G. Lũders, Det. Kon. Dan. Vid. Sel. Mat. -fys. Medd. **28**, 1 (1954); Ann. Phys. (N.Y.) **2**, 1 (1957); W. Pauli, in *Niels Bohr and the Development of Physics*, edited by W. Pauli (Pergamon Press, New York, 1955), p. 30; J. S. Bell, Proc. R. Soc. London, Ser. A **231**, 491 (1955); R. Jost, *The General Theory of Quantized Fields* (Am. Math. Soc., Providence, 1965).

[9] A. Einstein, Jahrb. Rad. Elektr. **4**, 411 (1907); C. M. Will, *Theory and Experiment in Gravitational Physics* (Cambridge University Press, Cambridge, 1981).

[10] G. Gabrielse *et al.*, Phys. Lett. B **455**, 311 (1999).

[11] D. P. Taylor, J. G. Goode, J. E. LeClaire, and P. M. Johnson, J. Chem. Phys. **103**, 14 (1995); A. Fujii, A. Iwasaki, T. Ebata, and N. Mikami, J. Phys. Chem. **101**, 5963 (1997); M. Gerhards, M. Schiwek, C. Unterberg, and K. Kleinermanns, Chem. Phys. Lett. **297**, 515 (1998).

[12] D. Wineland, P. Ekstrom, and H. Dehmelt, Phys. Rev. Lett. **31**, 1279 (1973).

[13] D. J. Wineland and H. G. Dehmelt, J. Appl. Phys. **46**, 919 (1974); G. Gabrielse, Phys. Rev. A **27**, 2277 (1983); C. S. Weimer, J. J. Bollinger, F. L. Moore, and D. J. Wineland, *ibid.* **49**, 3842 (1994).

[14] T. F. Gallagher, *Rydberg Atoms* (Cambridge University Press, Cambridge, UK, 1994).

[15] F. Robicheaux, C. Wesdorp, and L. D. Noordam, Phys. Rev. A **62**, 043404 (2000).

[16] T. J. Bensky, M. B. Campbell, and R. R. Jones, Phys. Rev. Lett. **81**, 3112 (1998).

[17] D. You *et al.*, Opt. Lett. **18**, 290 (1993); R. R. Jones, D. You, and P. H. Bucksbaum, Phys. Rev. Lett. **70**, 1236 (1993).

[18] H. L. Bethlem, G. Berden, A. J. A. van Roij, F. M. H. Crompvoets, and G. Meijer, Phys. Rev. Lett. **84**, 5744 (2000).